Available online at www.sciencedirect.com
SCIENCE DIRECT®
Journal of Sound and Vibration 274 (2004) 193–213
JOURNAL OF SOUND AND VIBRATION
www.elsevier.com/locate/jsvi

Smart panel with multiple decentralized units for the control of sound transmission. Part II: design of the decentralized control units

P. Gardonio*, E. Bianchi, S.J. Elliott

Institute of Sound and Vibration Research, University of Southampton, Highfield, Southampton SO17 1BJ, UK

Received 29 November 2002; accepted 20 May 2003

Abstract

This is the second of three companion papers that summarize the theoretical and experimental work carried out to develop a prototype smart panel with 16 decentralized vibration control units for the reduction of sound radiation/transmission. In this paper the design and implementation of the 16 decentralized control units is discussed. Each control unit consists of a collocated accelerometer sensor and piezoceramic patch actuator with a single channel velocity feedback controller in order to generate active damping.

The design and implementation of a single control unit has been discussed first. The frequency response function of the sensor–actuator pair has been measured and compared with the results of a computer simulation in order to investigate the effects of accelerometer dynamics, and actuator size. Since the system is only conditionally stable, a phase lag compensator has then been designed so that larger control gains that guarantee stability could be implemented.

The single-channel controller has then been implemented on each of the 16 decentralized control loops in the final system. The stability of the final control system has been assessed by plotting the 16 eigenvalues loci matrix product between the open loop sensors–actuators frequency response matrix and the diagonal matrix of control functions (fixed control gains multiplied by the phase lag compensators). None of the loci encircle the Nyquist point $(-1,0)$ as the frequencies varies from $-\infty$ to $+\infty$ at moderate gains, although part of the locus occupies the left hand side of the plot. Thus the complete control system is stable only for a limited range of control gains.

The control effectiveness of both the single control unit and 16 decentralized control units has been assessed by plotting the velocity at one error sensor with reference to either an acoustic source in the cavity (loudspeaker) or a primary point force on the panel (shaker).

*Corresponding author. Tel.: +44-23-8059-4933; fax: +44-23-8059-3190.
E-mail address: pg@isvr.soton.ac.uk (P. Gardonio).

0022-460X/$ - see front matter © 2003 Elsevier Ltd. All rights reserved.
doi:10.1016/j.jsv.2003.05.007

1. Introduction

This is the second of three companion papers that summarize the theoretical and experimental work carried out to develop a prototype smart panel with 16 decentralized vibration control units for the reduction of sound radiation/transmission. The system studied consists of a thin aluminium panel of dimensions $414 \times 314\,\text{mm}^2$ and thickness 1 mm with an embedded array of 4×4 square piezoceramic PZT (lead, zirconate, titanate) actuators. The sensing system equally consists of an array of 4×4 accelerometers that are arranged in such a way as to match the centre positions of the 16 piezoceramic patches. Each of the 16 sensor–actuator pairs is set to implement decentralized velocity feedback control, e.g. active damping [1]. The theoretical study in Part I [2] has shown that, with this arrangement, both the kinetic energy of the panel and its transmitted/radiated sound power can be significantly reduced in the bandwidth up to 2 kHz provided an appropriate feedback gain is chosen.

In this paper the design and implementation of the 16 decentralized feedback control units is discussed. The first part of the paper describes the design study of the single channel velocity feedback control loop in the case where only one control unit is working. In Section 2 the open loop sensor–actuator measured frequency response function of the active control unit is analyzed and contrasted with that derived from simulations in a frequency range up to 50 kHz. This study is primarily focussed to assess whether the accelerometer sensor and piezoceramic patch actuator are collocated and dual in which case it would be possible to implement unconditionally stable direct velocity feedback [3–7]. For the theoretical study, the mobility-impedance model presented in Part I [2] is used. With this model the passive dynamic effects of the 16 sensors and actuators are taken into account and the response of the panel is fully coupled to the acoustic field in the cavity. The dynamic effects due to the size and stiffness/weight of the piezoceramic patch actuator as well as the effects due to the weight and mounted fundamental resonance of the accelerometer sensor have been investigated. The coupling of the piezoceramic patch actuator with the panel has also been investigated in detail by measuring with a laser vibrometer the response of the panel at specific frequencies in the vicinity of the actuator. The Nyquist stability criterion [1] has then been used to finalize the design of the controller. In Section 3 both the design of a fixed gain velocity feedback controller with and without a phase lag compensator are presented. Finally in Section 4 the control effectiveness of the single working unit is shown by plotting the velocity measured at the error sensor with and without velocity feedback control when the panel is excited either by the acoustic source in the cavity (loudspeaker) or the point force on the panel (shaker).

The second part of the paper discusses the implementation of the 16 decentralized velocity feedback control units with the phase lag compensator designed in Section 3 with reference to just one working control unit. Elliott et al. [3] have shown that when the 16 decentralized control units consist of collocated and compatible sensor–actuator pairs [4–7] then the system is proven to be unconditionally stable at any frequency. Since the accelerometer and piezoceramic patch sensor–actuator pairs are not collocated and dual, the control stability of the system with 16 control units has been assessed in Section 5 by considering the loci of the eigenvalues of the matrix product between the open loop sensors–actuators transfer matrix and the diagonal matrix of control functions (fixed control gains multiplied by the phase lag compensators) [3,8]. In a similar way to the Nyquist stability criterion, the stability of the multi-channel control system is guaranteed if none of the eigenvalues encloses the Nyquist point $(-1,0)$ as the frequencies vary

from $-\infty$ to $+\infty$ [8]. The control effectiveness of the 16 control units has then been assessed by plotting the velocity measured at one error sensor with and without the 16 velocity feedback controls when the panel is excited either by the acoustic source in the cavity (loudspeaker) or the point force on the panel (shaker).

2. Open loop sensor–actuator measured/simulated frequency response function

In this section the measured and the simulated frequency response functions of the sensor–actuator pair number 7 in Fig. 1 are analyzed. For these measurements the panel has been mounted on the rectangular cavity with rigid walls which is described in more detail in Part III [9]. Also the response of the panel in the vicinity of a piezoceramic patch actuator is considered at specific frequencies in such a way as to study the coupling between the actuator and the panel.

The measured frequency response function has been compared with the simulated one, which has been derived using the mathematical model presented in Part I [2]. When the dynamic effects of the 16 sensor–actuator systems are taken into account and no primary excitation is present in the cavity or applied to the panel, i.e. $\mathbf{q}_p(\omega) \equiv \mathbf{0}$ and $\mathbf{f}_p(\omega) \equiv \mathbf{0}$, then, according to Eqs. (37) and (32) in Part I [2] the relation between the 16 measured velocities at the error sensor positions, $\mathbf{v}_m(\omega)$, and the control excitations of the 16 piezoceramic patches, $\mathbf{f}_s(\omega)$ is given by

$$\mathbf{v}_m(\omega) = \mathbf{T}_{ms}(\omega)\mathbf{f}_s(\omega), \tag{1}$$

where $\mathbf{T}_{ms}(\omega) = \mathbf{A}(\omega)\mathbf{T}_{cs}(\omega)$ and the $\mathbf{A}(\omega)$ and $\mathbf{T}_{cs}(\omega)$ matrices are given by Eqs. (38) and (33f) in Part I [2]. The transfer matrix $\mathbf{T}_{cs}(\omega)$ accounts for both the passive effect of the acoustic cavity on which the panel is mounted and the dynamics effects of the 16 piezoceramic patch and accelerometer transducers. As shown in Fig. 2 the dynamics of each sensor–actuator unit has been modelled with three lumped elements: (a) a bottom mass that includes part of the piezoceramic actuator mass and the mass of the accelerometer case; (b) a lumped spring and damper for the piezoceramic element in the accelerometer, and (c) the inertial mass of the accelerometer. The dynamic effects of the piezoceramic actuator have been smeared over the panel surface by modifying the Young's modulus and density parameters of the panel.

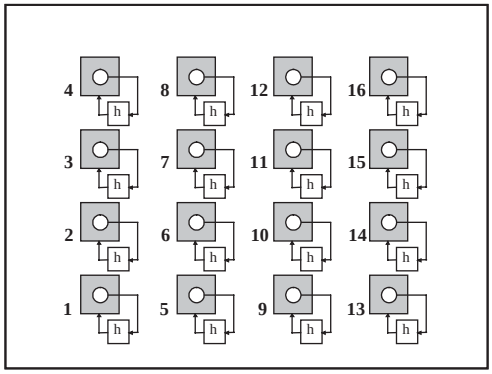

Fig. 1. Arrangement of 16 piezoceramic actuators, as shown by the squares, driven locally by the output of 16 velocity sensors, as shown by the circles, via individual control loops with a gain of h.

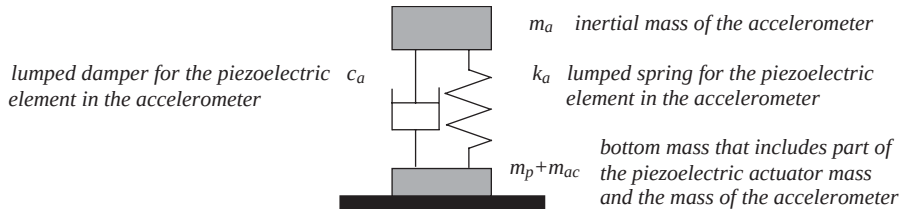

Fig. 2. Schematic representation of one sensor–actuator system.

Table 1
Physical properties of the sensor–actuator transducers

Parameter	Value
Mass of the piezo actuator	$m_p = 0.2 \times 10^{-3}$ kg
Mass of the accelerometer case	$m_{ac} = 0.2 \times 10^{-3}$ kg
Inertia mass of the accelerometer	$m_a = 0.22 \times 10^{-3}$ kg
Stiffness of the accelerometer	$k_a = 1.1 \times 10^7$ N/m
Mounted resonance frequency of accelerometer	$f_a = \omega_n/2\pi = 33.6 \times 10^3$ Hz
Damping coefficient of the accelerometer	$c_a = 2.5$ N/m s^{-1}

The 16 sensor–actuator frequency response functions can be extracted from Eq. (1) by taking the 16 diagonal terms of the matrix $\mathbf{T}_{ms}(\omega)$. For example the frequency response function giving the measured velocity at the accelerometer sensor number 7 due to the unit excitation of the collocated piezoceramic actuator number 7 is given by the frequency response function $T_{ms7,7}(\omega)$.

In practice the physical properties of the 16 accelerometer sensors and piezoceramic actuators differ from each other, in particular each accelerometer has a different resonance frequency which, for the 16 transducers used in the smart panel, have been found to go from a minimum of 35 kHz to a maximum of about 42 kHz. This variability of the resonance frequency is rather important and therefore the simulations shown below have been obtained by using the physical parameters summarized in Table 1 with the inertia masses of the 16 accelerometers, m_a, spread in a range of values such that the natural frequencies of the 16 accelerometers are uniformly distributed between 35 and 42 kHz. Also, in order to account for the inertia and stiffening effects of the piezoceramic actuators the smeared density $\bar{\rho}_s = 3000$ kg/m^3 and smeared Young's modulus of elasticity $\bar{E}_s = 7.1 \times 10^{10}$ N/m^2 have been used in the simulations of the panel response.

In Figs. 3–5, the measured sensor–actuator frequency response functions are contrasted with those obtained from the numerical model respectively for three frequency ranges of 0–1, 0–10 and 0–50 kHz. In these plots, together with the measured frequency response function (faint line) two other curves are plotted: the first is the simulated sensor–actuator frequency response function when the sensor–actuator mass and dynamics effects are not accounted for (dashed line), and the second is the simulated sensor–actuator frequency response function when the sensor–actuator mass and dynamics effects are instead taken into account (solid line).

Fig. 3 shows that, for frequencies up to the sixth resonance frequency of the plate (283 Hz), the solid line, which represents the simulated frequency response function with the sensor–actuator

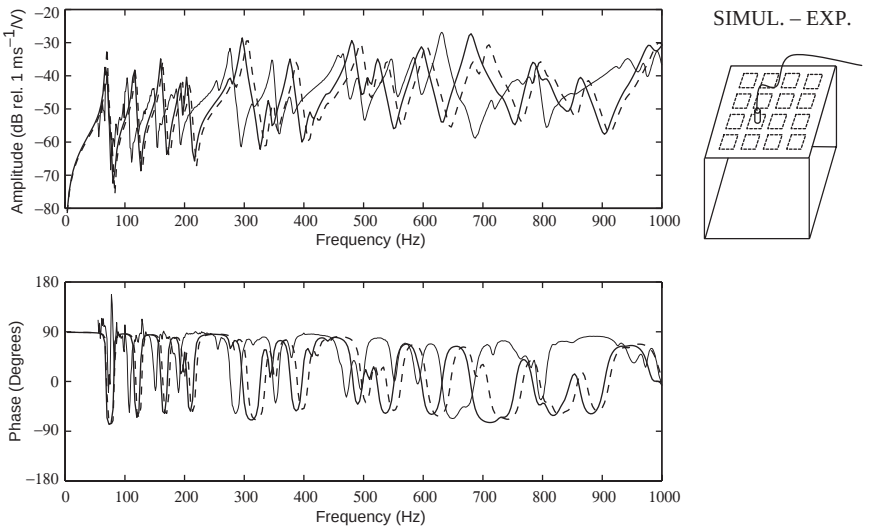

Fig. 3. Open loop frequency response function (0–1 kHz) of the sensor/actuator pair number 7. Simulated FRF with no effects (dashed line), with sensor–actuator mass and dynamics effects (solid line), and measured FRF (faint line).

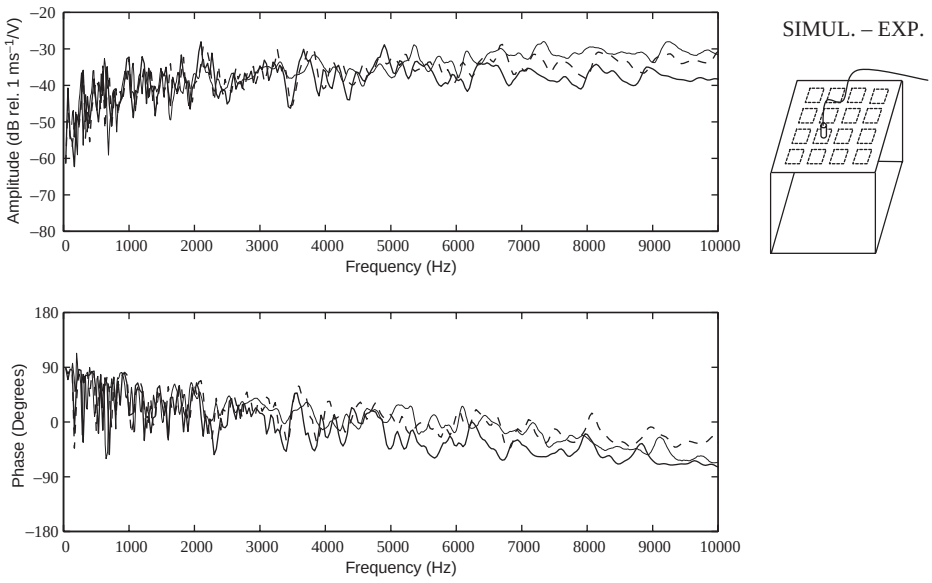

Fig. 4. Open loop frequency response function (0–10 kHz) of the sensor/actuator pair number 7. Simulated FRF with no effects (dashed line), with sensor–actuator mass and dynamics effects (solid line), and measured FRF (faint line).

dynamic effects, overlaps the dashed line, which represents the simulated frequency response function without the sensor–actuator mass and dynamics effects. However, for frequencies above the sixth resonance, the sensor–actuator dynamic effect produces a small downward shifting of the resonance frequencies of the plate as one would expect with an increment of the mass.

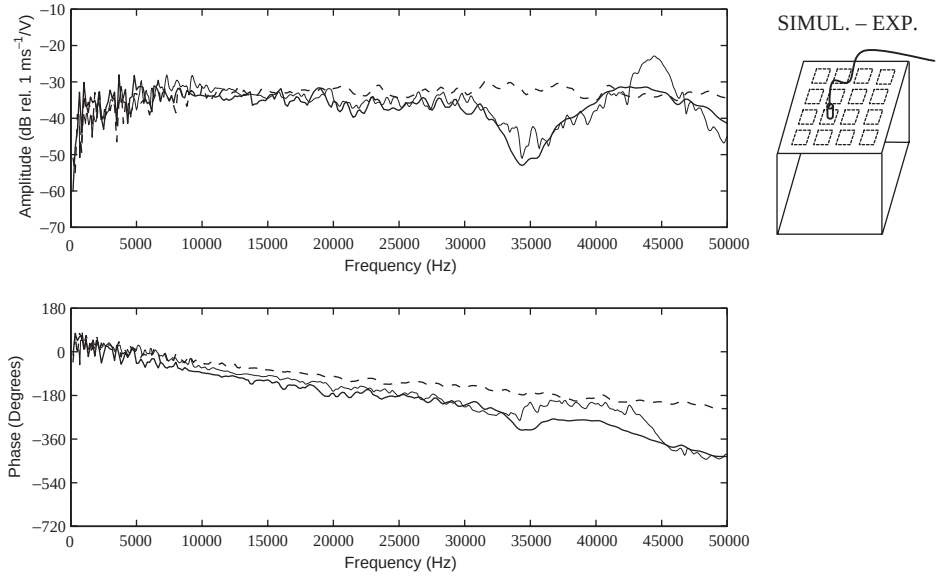

Fig. 5. Open loop frequency response function (0–50 kHz) of the sensor/actuator pair number 7. Simulated FRF with no effects (dashed line), with sensor–actuator mass and dynamics effects (solid line), and measured FRF (faint line).

Comparing the measured frequency response function with the numerical simulation when the dynamic effects of the sensor–actuator transducers are taken into account, it can be seen that the agreement between the experimental and numerical results is relatively good up to 200 Hz and can be considered satisfactory at higher frequencies. The measured frequency response function is well reproduced by the simulation except for a shift in frequency that is probably due to the uncertainty for some of the parameter used to model the dynamic effects of the actuator and sensor transducers.

Fig. 4 shows the two simulated frequency response functions compared with the measured frequency response function in a frequency range of 0–10 kHz. Above 4 kHz, the amplitude of the simulated frequency response function with sensor–actuator dynamics effects of the transducers (solid line) presents a more flat trend of the module with respect to the simulated frequency response function, which does not account for these effects (dashed line). In terms of amplitudes, both simulated curves present small differences with respect to the measured one (faint line) and in terms of phase values a good agreement can be seen, particularly between the measured and simulated frequency response functions which include the sensor–actuator effects.

Fig. 5 shows the two simulated frequency response functions compared with the measured frequency response function in a frequency range of 0–50 kHz. The simulated frequency response function that does not account for the sensor–actuator dynamics effects of the transducers (dashed line) presents an almost flat amplitude trend in the whole frequency range. In contrast, the frequency response function which takes into account both the accelerometer and piezoceramic actuator mass effects and the accelerometer dynamics (solid line) has a more complex behaviour which is characterized by a relatively wide frequency band trough between 30 and 40 kHz and a crest between 43 and 46 kHz which better agrees with the measured response.

As shown in Fig. 2, the accelerometer can be considered as a single-degree-of-freedom neutralizer that reduces the vibration level at the measurement point in correspondence to its natural frequency. In fact each input impedance frequency function of the accelerometers has a peak in correspondence to the resonance frequency of the accelerometers and then a trough at higher frequencies. Fig. 6 shows the simulated input impedances of the 16 accelerometers with the physical parameters given in Table 1 with variable inertia mass so that their resonance frequencies are uniformly spread between 35 and 42 kHz. From this plot it is evident that there is a relatively high impedance effect at the frequency band of the resonances that tends to reduce the vibration of the panel as found in Fig. 5.

The sensitivity functions that give the ratio between the measured velocity signals by the accelerometers and the true velocities underneath the accelerometers are characterized by a peak in correspondence to the resonance frequencies of the accelerometers. However, for each accelerometer, this effect is limited to a relatively narrow frequency band as shown in Fig. 7 for the accelerometer number 7. Therefore, the measured sensor–actuator frequency response function remains characterized by the trough at 30–40 kHz and the crest between 43 and 46 kHz generated by the 16 accelerometers that work as neutralizers.

The analysis of the measured and simulated sensor–actuator frequency response functions shows that the frequency responses are affected by a phase lag greater than -90° above 10 kHz as shown for example in Fig. 5. This phase lag is probably due to both electric delay in the measurement chain (accelerometer, cables, signal conditioning system) and to the fact that the accelerometer and the piezoceramic patch are not a truly collocated and dual sensor–actuator pair. The actuation mechanism of the piezoceramic actuator can be modelled as four lines of moments acting along the edges of the piezoceramic patch [10]. The sensor is instead measuring the transverse velocity at the centre position of the actuator patch. There are thus two types of

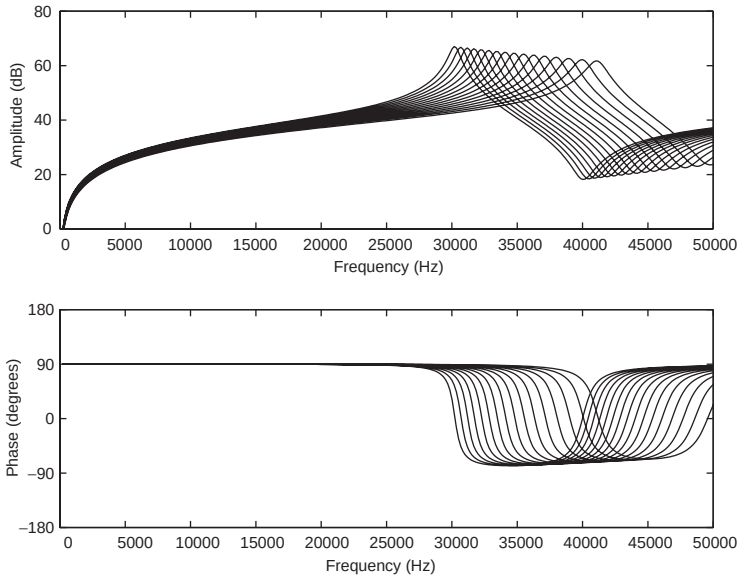

Fig. 6. Input impedance functions of the 16 accelerometer sensors used in the numerical model for the response of the smart panel.

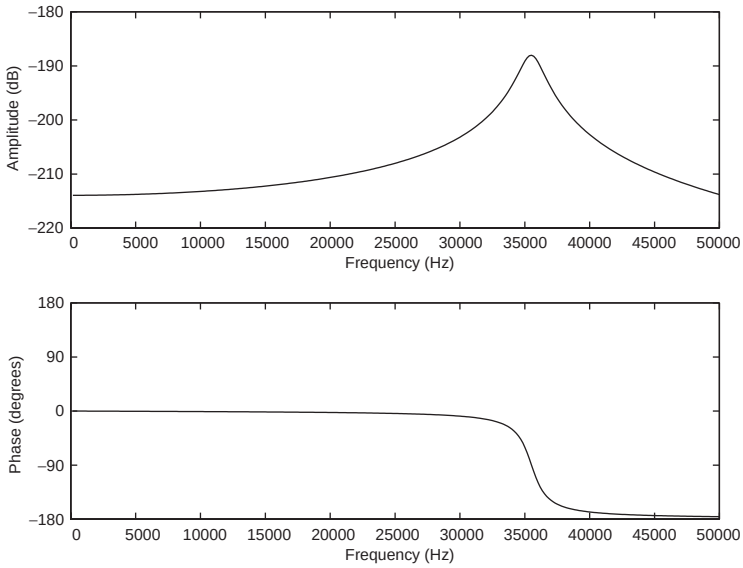

Fig. 7. Sensitivity function of one accelerometer used in the numerical model for the response of the smart panel.

problems: the actuation and sensing are not collocated and also the moment actuation is not compatible to the linear transverse velocity sensing. Both effects contribute to determine a non-positive definite frequency response function at higher frequencies [4–7].

The non-collocated positioning effect found above 10 kHz for the accelerometer sensor and piezoceramic actuator frequency response function partly depends on the size of the actuator patch with reference to the bending wavelength vibration of the plate. The collocated positioning effect can therefore be extended to a wider frequency range by using a smaller piezoceramic patch actuator. Fig. 8 shows the predicted sensor–actuator frequency response functions with two different piezoceramic patch actuators, of dimensions $25 \times 25\,\mathrm{mm}^2$ (solid line) and $12 \times 12\,\mathrm{mm}^2$ (faint line). The bottom plot confirms that with a smaller patch the phase roll off is much lower than with the larger patch. Indeed by halving the size of the actuator the real part of the frequency response function is then found to be positive definite up to about 35 kHz. The drawback is that by reducing the size of the piezoceramic patch the control authority is also decreased. Therefore, a compromise has to be found between the possibility of extending the minimum phase property of the sensor–actuator frequency response function to higher frequencies and the required control authority to produce the desired control effect.

In order to investigate the behaviour of the piezoceramic actuator at the high frequencies, a further analysis of the vibration level around a sensor–actuator pair has been carried out using a Laser Doppler Vibrometer (LDV). The system has been excited with a random signal up to 50 kHz directly applied to the tested piezoceramic actuator patch. A grid of 480 points to be scanned has been defined on a square surface of the piezo patch centred with respect to the accelerometer sensor and a set of frequency response functions between the velocity at each grid point and the primary disturbance has been measured by means of the laser vibrometer. This set of data has been processed by the laser software system in order to obtain two-dimensional (2-D)

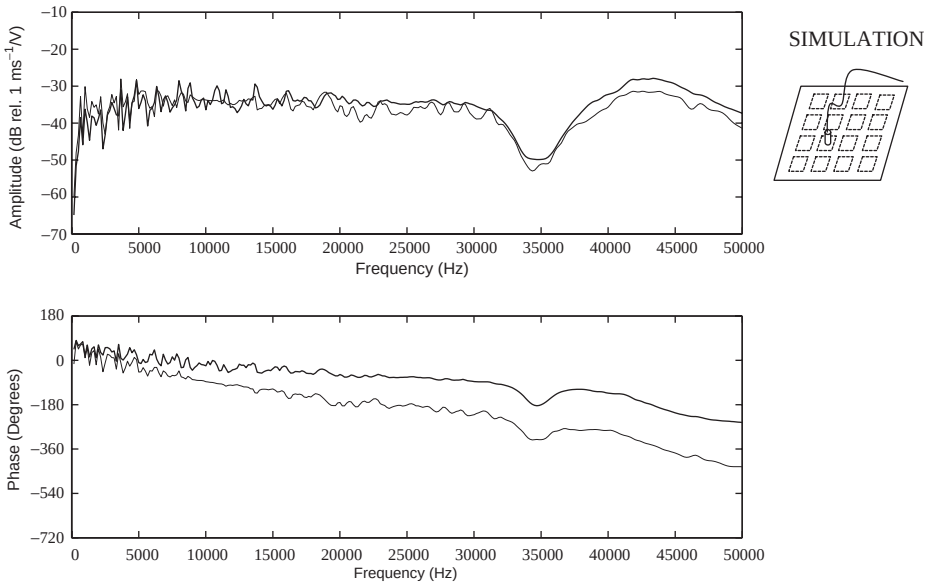

Fig. 8. Open loop frequency response function (0–50 kHz) of the sensor/actuator pair number 7. Simulated FRF with standard size piezoceramic patch (solid line) and with smaller size patch (faint line).

colour coded images of the velocity distribution around the sensor–actuator pair at different frequencies, as shown in the plots below.

Fig. 9 shows the distribution of the vibration velocity of the scanned area around the sensor at 343 Hz (a), 2.116 kHz (b), 16.09 kHz (c) and 44.13 kHz (d). Considering the top two Figs. 9a and b, the vibration level is uniformly distributed on the scanned area since the wavelength of the bending wave is bigger than the actual size of the piezo patches. For frequencies such that the bending wavelength is shorter than the dimension of the piezoceramic patch, the distribution of velocity becomes less uniform, as shown in Figs. 9c and d for the frequencies of 16 kHz (left side picture) and 44 kHz (right side picture). At such higher frequencies the bending wavelengths are shorter than the piezo dimensions. Also, the various components of the sensor–actuator transducers behave less and less as "lumped parameter" elements and therefore directly affect the overall vibration of the panel in the vicinity of the control unit. As explained above, at these frequencies the sensor–actuator pair cannot be considered to be truly collocated with the consequence of a non-positive definite real part frequency response function. It is interesting to note that in all plots there is no discontinuity of the measured velocity around the edges of the piezoceramic patch. It seems that neither the stiffening and mass passive effects nor the actuation in-plane deformation effect of the piezoceramic patch produce relevant discontinuities of the transverse vibration around it.

3. Design of a single feedback control system

The design of the single channel velocity feedback control systems has been tested on the sensor–actuator pair number 7 when the panel is mounted on the rectangular cavity which is

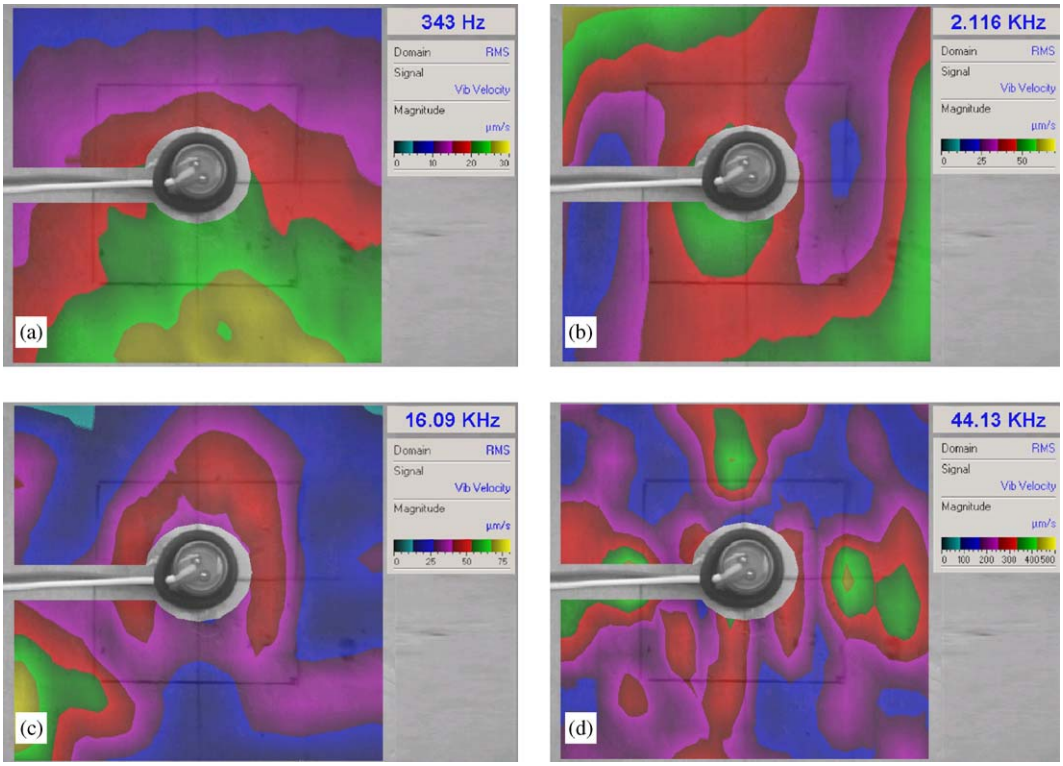

Fig. 9. Vibration velocity of the plate in correspondence of a sensor–actuator pair, assessed with the laser vibrometer and using the piezo actuator as primary excitation. 343 Hz (a), 2.116 kHz (b), 16.09 kHz (c), 44.13 kHz (d).

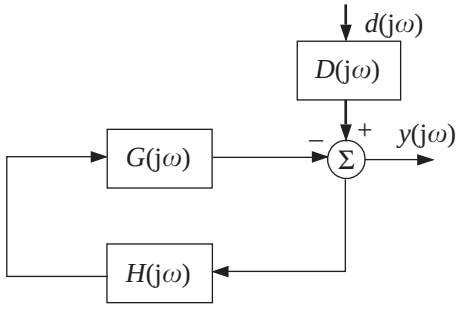

Fig. 10. Block diagram of the closed loop feedback control system.

described in more details in Part III [9]. Fig. 10 shows the block diagram of the single-input single-output feedback control system that has been implemented. The total output velocity measured by the accelerometer sensor, $y(j\omega)$, is given by the vibration generated by the primary disturbance, $d(j\omega)$, which can be either the acoustic source in the cavity underneath the panel (loudspeaker) or the primary force acting on the panel (shaker), and by the vibration generated by the control actuator which is set to be proportional, but with opposite phase, to the velocity measured by the

accelerometer sensor itself. Assuming that this feedback control scheme is stable, the ratio between the error signal, $y(j\omega)$, and that of the primary disturbance, $d(j\omega)$, is given by [1]

$$\frac{y(j\omega)}{d(j\omega)} = \frac{D(j\omega)}{(1 + G(j\omega)H(j\omega))}, \tag{2}$$

where $G(j\omega)$ is the frequency response function between the sensor and actuator pair, $D(j\omega)$ is the frequency response function between the sensor and the excitation source (loudspeaker or shaker) and $H(j\omega)$ is the control function.

As shown in Fig. 10, in order to implement velocity feedback control, the control function is set to be a constant gain $H(j\omega) = h$ so that, provided the real part of the sensor–actuator frequency response function is positive real, by increasing the gain h the ratio $y(j\omega)/d(j\omega)$ is always brought down. In order to guarantee an unconditionally stable control operability that gives reductions of vibration at all frequencies, the Nyquist plot of the open loop frequency response function

$$L(j\omega) = G(j\omega)H(j\omega) \tag{3}$$

should stay in the right-hand half of the complex plane for any frequency [1]. The analysis presented in the previous section has shown that the frequency response function of the sensor–actuator pair is not minimum phase. Indeed above about 10 kHz the phase exceeds -90° and constantly rises up to -270° in correspondence to 48 kHz. Also, the amplitude gradually rises up to 2 kHz and then remains constant around the maximum amplitude values at higher frequencies. There is just a trough between 30 and 40 kHz, which is however followed by a crest with relatively high amplitudes between 43 and 46 kHz. Therefore it is likely that at higher frequencies the sensor–actuator frequency response function enters the left-hand side of the Nyquist plot and, for relatively low values of gains, goes into the circle of radius 1 and centre $(0, -1)$ or even encircles the Nyquist point $(0, -1)$ since the amplitude of the sensor–actuator response was found to be relatively large even at high frequencies. Thus, it is possible that even for small values of gain the control system is affected by control spillover at the higher frequencies or even goes unstable [1].

Fig. 11(a) shows the Nyquist plot of the open loop frequency response function from 5 kHz to 50 kHz for a constant control gain $H(j\omega) = 30$. This plot is focussed on higher frequency response in order to asses the stability of the controller. The low frequency part of the transfer function has been omitted to avoid overcomplicating the graph. The trough of the amplitude of the sensor–actuator frequency response function between 30 and 40 kHz, which is due to the neutralizing effects of the 16 accelerometers, occupies exactly the negative, left-hand side, of the Nyquist plot. Therefore, as expected the Nyquist plot is characterized by a left-hand side part which however is quite squeezed towards the imaginary axis. This is a very important result, since, even if the sensor–actuator frequency response function is not minimum phase, relatively large control gains could still be implemented without entering into instability and without having too large control spillover phenomena at relatively higher frequencies. Also, the resonance effect due to the accelerometer sensor at around 44 kHz is, in this case, not compromising the stability of the control system since the sensor–actuator frequency response function between 40 kHz and about 50 kHz is positive definite. It must be said that this type of sensor–actuator response function was not designed in advance and has come out from a happy choice of the accelerometer and the mass of the piezoceramic patch. Since it is very difficult to construct a collocated and dual sensor–actuator pair at all frequencies, it is then very important to design the two transducers in

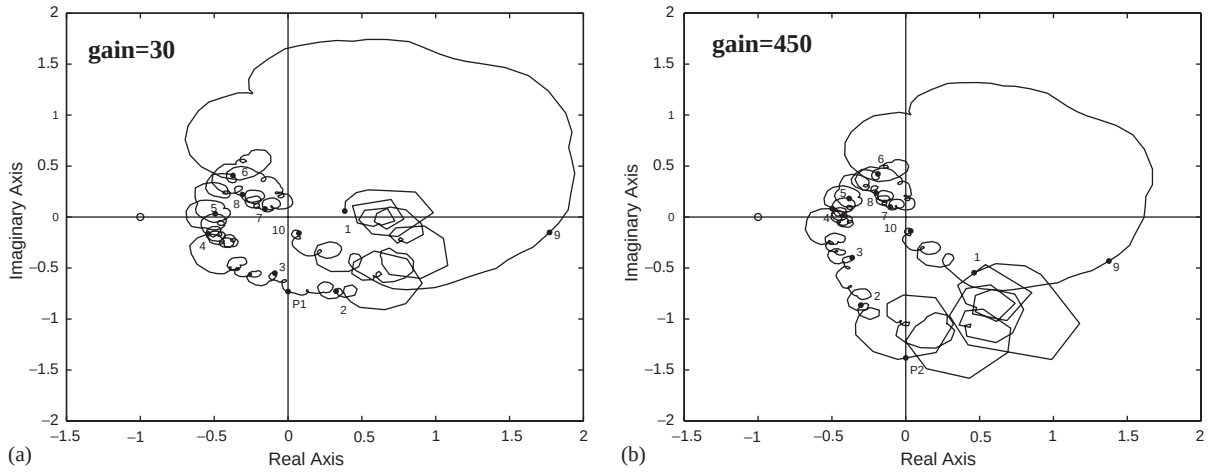

Fig. 11. Nyquist plot of the frequency response function between 5 and 50 kHz of the sensor number 7, exciting with the collocated piezoceramic actuator: 1 = 5 kHz, 2 = 10 kHz, 3 = 15 kHz, 4 = 20 kHz, 5 = 25 kHz, 6 = 30 kHz, 7 = 35 kHz, 8 = 40 kHz, 9 = 45 kHz, 10 = 50 kHz; (a) without compensator (gain of 30, $P1 = 12.5$ kHz); (b) with compensator (gain of 450, $P2 = 9.25$ kHz).

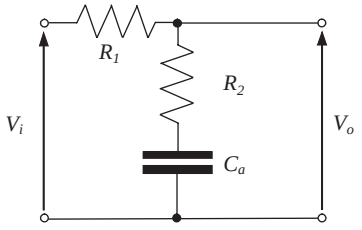

$$C(\mathrm{j}\omega) = \frac{V_o(\mathrm{j}\omega)}{V_i(\mathrm{j}\omega)} = \frac{1 + \mathrm{j}\omega R_2 C_a}{1 + \mathrm{j}\omega(R_1 + R_2)C_a}$$

$R_1 = 18\ \mathrm{k}\Omega$
$R_2 = 1\ \mathrm{k}\Omega$
$C_a = 15\ \mathrm{nF}$

Fig. 12. Phase-lag compensator built in the feedback controller.

such a way that the Nyquist plot of the sensor–actuator response function has a small negative real part.

As discussed above, the test panel studied for one control unit is prone to generating instabilities in a frequency range between 12.5 and 40 kHz. Therefore, in order to give the possibility of implementing the high gains required to obtain the wanted reductions of the vibration and sound radiation of the panel, the phase-lag compensator with frequency response function $C(\mathrm{j}\omega)$, shown in Fig. 12, has been designed and implemented in the controller that is shown in Fig. 10. The optimal values for the resistors and capacitor of the compensator circuit have been derived iteratively by simulating the open loop frequency response function $L'(\mathrm{j}\omega) = G(\mathrm{j}\omega)H'(\mathrm{j}\omega)$ where

$$H'(\mathrm{j}\omega) = hC(\mathrm{j}\omega) \tag{4}$$

and $C(\mathrm{j}\omega)$ is the phase-lag compensator which, according to the notation given in Fig. 12, is given by

$$C(\mathrm{j}\omega) = \frac{V_o(\mathrm{j}\omega)}{V_i(\mathrm{j}\omega)} = \frac{1 + \mathrm{j}\omega R_2 C_\mathrm{a}}{(1 + \mathrm{j}\omega(R_1 + R_2)\mathrm{C_a})}. \tag{5}$$

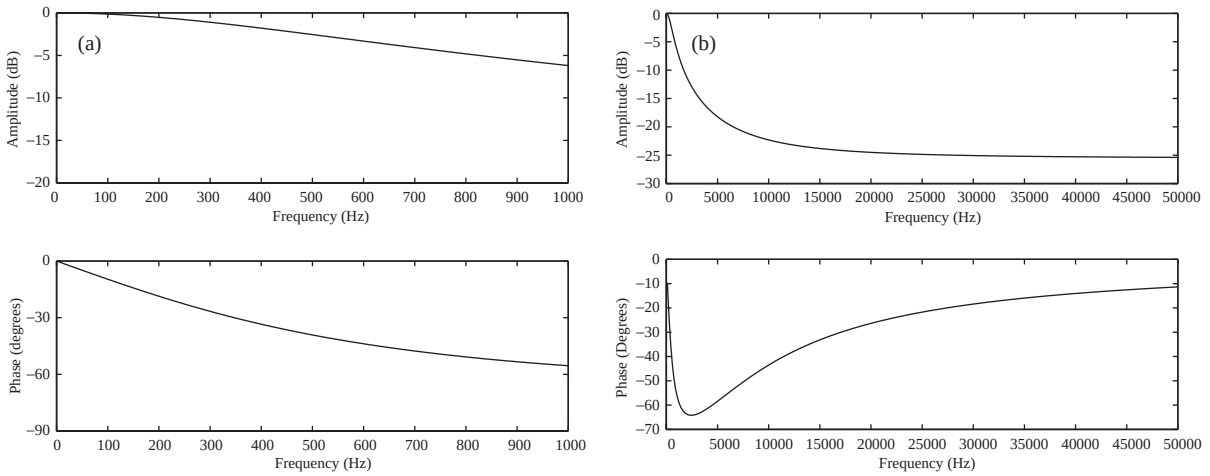

Fig. 13. Transfer function of the compensator in the range 0–1 kHz (a) and 0–50 kHz (b).

The iterative procedure has been brought to the design of a phase-lag compensator with the resistors $R_1 = 18\,\mathrm{k\Omega}$ and $R_2 = 1\,\mathrm{k\Omega}$ and capacitor $C_a = 15\,\mathrm{nF}$. As shown in Fig. 13, this compensator has a relatively large amplitude roll off with a phase lag up to -65° at 3 kHz, which is recovered at higher frequencies. Fig. 11(b) shows the Nyquist plot of the open loop frequency response function $L'(j\omega)$ from 5 to 50 kHz with the compensator in Fig. 12 and a control gain $H(j\omega) = 450$. This figure shows how the compensator has rotated the Nyquist plot in a clockwise direction such that the real part of the transfer function $L'(j\omega)$ enters the negative side of the plot at 9.5 kHz to leave it at about 40 kHz. However, comparing this plot with that relative to the implementation of direct velocity feedback in Fig. 11(a), it can be noticed that the same stability margin is achieved with the compensator as in the case of direct velocity feedback but with a 15 times higher control gain. It should be noted that the Nyquist plots in Fig. 11 do not show the sensor–actuator frequency response function below 5 kHz which, according to Figs. 4 and 5, is positive definite with higher amplitude than the crest between 43 and 46 kHz and thus it occupies the right-hand side of the Nyquist plot and it exceeds the limits of the real and imaginary axes in the two plots.

4. Implementation of a single feedback control system

The practical implementation of the feedback control system number 7 in Fig. 1 is now discussed. This experimental work has been carried out with the panel mounted on the rectangular cavity with rigid walls which is described in Part III [9]. The control effectiveness of the system has been assessed with reference to two primary excitations: first the acoustic source in the cavity (loudspeaker) and second, the point force on the panel (shaker).

The two plots in Fig. 14 show the measured velocity at error sensor number 7 per unit excitation of the loudspeaker in the cavity between 0–1 (a) and 0–2 (b) kHz without control (solid line) and when the feedback control system with compensator number 7 is implemented using a

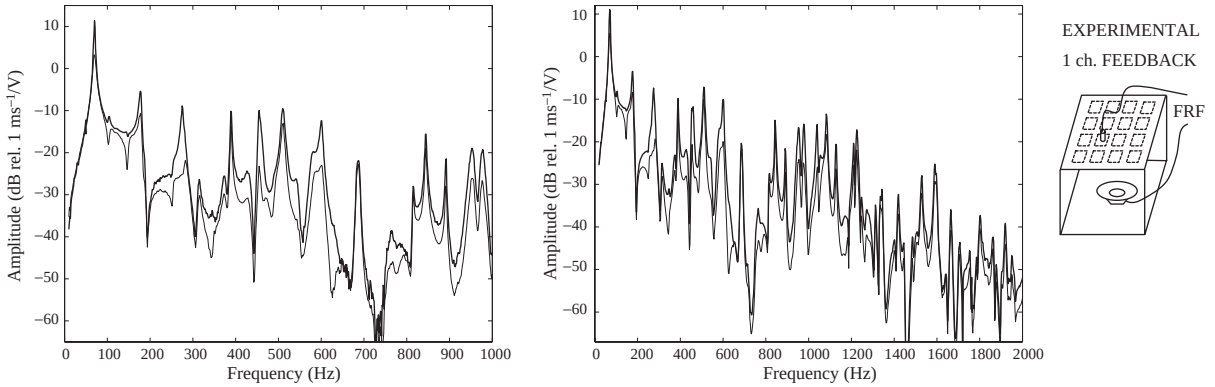

Fig. 14. Measured velocity at error sensor number 7 per unit excitation of the loudspeaker in the cavity between 0–1 (a) and 0–2 (b) kHz without control (solid line) and when the feedback control system with compensator number 7 is implemented (faint line).

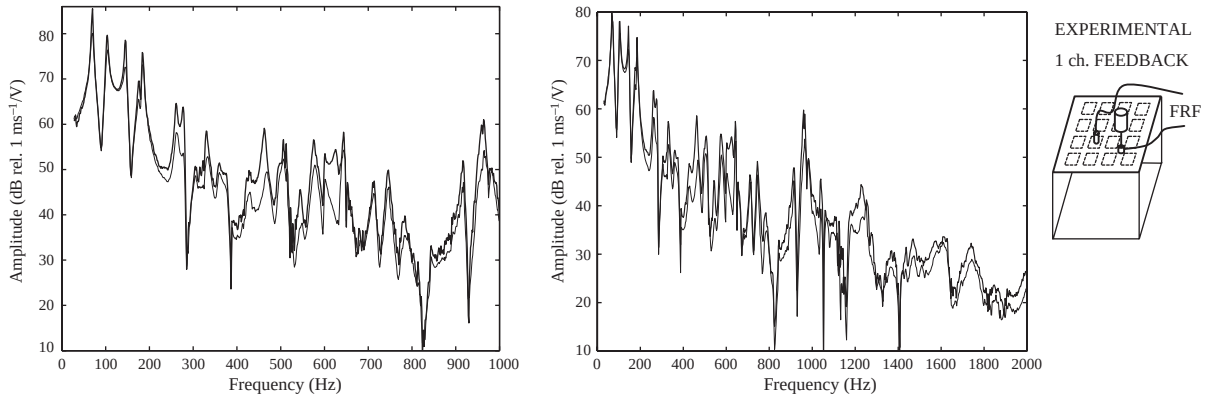

Fig. 15. Measured velocity at error sensor number 7 per unit excitation of the shaker on the panel between 0–1 (a) and 0–2 (b) kHz without control (solid line) and when the feedback control system with compensator number 7 is implemented (faint line).

relatively high gain that nevertheless guarantees stability (faint line). These two plots indicate that good reductions of the vibration level are achieved up to 2 kHz. Considering Fig. 14(a) in more detail it can be noticed that the control system finds rather difficult to damp down the resonance frequencies at 70, 177, 388, 510, 686, 844 and 892 Hz. This is due to three possible factors: first, the loading effect on the panel generated by the low frequency volumetric acoustic response of the cavity; second, the low spatial control authority of the sensor–actuator number 7 for some of the resonant structural modes and third, the low control strength of the sensor–actuator number 7 for well coupled panel and cavity modes. Moreover, the piezoceramic patch actuator does not efficiently excite the low frequency bending modes of the panel because it produces moment excitations [11]. However, except for these modes, reductions from 5 up to 15 dB are measured up to 1 kHz. Also, considering Fig. 14(b), at higher frequencies still reductions up to 6 dB are measured within few narrow frequency bands.

The two plots in Fig. 15 show the measured velocity at error sensor number 7 per unit excitation of the shaker on the panel between 0–1 (a) and 0–2 (b) kHz without control (solid line) and when the feedback control system with compensator number 7 is implemented using a relatively high gain that guarantees stability (faint line). These two plots indicate similar results to those found for the loudspeaker primary excitation with relatively larger reductions of the vibration level up to 2 kHz. Fig. 15(a) shows that also in this case the control system finds it rather difficult to damp down some low frequency resonances particularly those at 70, 103, 183, 506, 643, 714 and 745 Hz mainly because of the low spatial control authority given by the single acting control unit. Except for these resonances, reductions from 5 up to 15 dB are measured up to 1 kHz and reductions of about 4 dB are found for a wide frequency band between 1200 and 2000 Hz.

5. Implementation of 16 decentralized single channel feedback control systems

In this section the implementation of the 16 velocity feedback control units with the phase-lag compensator designed in Section 3 for only one working control system is discussed both in terms of stability and control effectiveness. The 16 decentralized control units are arranged into a 4×4 grid as shown in Fig. 1. The block diagram of this multi-channel feedback control system is shown in Fig. 16. For this particular case, where the number of actuators and sensors is equal, the matrix with the transfer functions between the sensors and the actuators, $\mathbf{G}(j\omega)$, is square and, because the 16 control units are decentralized, the matrix with the feedback control functions $\mathbf{H}(j\omega)$ is diagonal and equal to the identity matrix multiplied by the control functions given by Eq. (4). The same control gain h and the phase-lag compensator have been implemented in each of the 16 feedback controllers. Provided the control system is stable, the vector with the residual signals at the sensor outputs, $\mathbf{y}(j\omega)$, is related to that of the primary excitations $\mathbf{d}(j\omega)$, by the expression

$$\mathbf{y}(j\omega) = [\mathbf{I} + \mathbf{G}(j\omega)\mathbf{H}(j\omega)]^{-1}\mathbf{D}(j\omega)\mathbf{d}(j\omega), \tag{6}$$

where $\mathbf{D}(j\omega)$ is the transfer matrix between the error sensors and the primary excitation $\mathbf{d}(j\omega)$. As mentioned in Section 3 the accelerometer sensor and piezoceramic patch actuator are not collocated and dual and thus the control system is not guaranteed to be unconditionally stable at all frequencies. The stability of the multi-channel decentralized feedback control system has

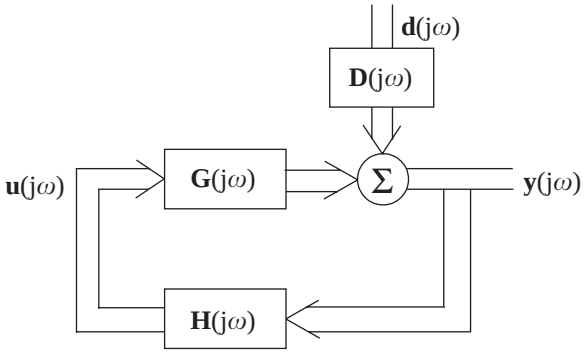

Fig. 16. Block diagram of the multichannel decentralized velocity feedback control system.

therefore been assessed by examining if the locus of the 16 eigenvalues of the matrix $\mathbf{G}(j\omega)\mathbf{H}(j\omega)$ encloses the Nyquist point $(-1,0)$ as ω varies from $-\infty$ to $+\infty$ [8]. This has required the measurement of the 16×16 sensor actuator frequency response functions. Fig. 17 shows the modulus of the 16 measured response functions between the 16 sensors and the actuator number 7 including the effect of the control function $hC(j\omega)$. Sixteen sets of these measurements were taken to build the complete sensors–actuators transfer matrix $\mathbf{G}(j\omega)\mathbf{H}(j\omega)$ in a frequency range 0–50 kHz [12]. With this set of data, the locus of the 16 eigenvalues of the matrix $\mathbf{G}(j\omega)\mathbf{H}(j\omega)$ have been calculated numerically and plotted in Fig. 18 in a frequency range between 5 and 50 kHz. Also in this case the low frequency part of the plots has been omitted to avoid overcomplicating the graph. It can be noticed that none of these loci encircles the Nyquist point $(-1,0)$ which proves that all 16 control units are stable for the given control gain.

As done for the single working control unit, the testing of the 16 decentralized control units has been carried out with the panel mounted on the rectangular cavity with rigid walls which is described in Part III [9]. Also, the control effectiveness of the system has been assessed with reference to two primary excitations: first the acoustic source in the cavity (loudspeaker) and second, the point force on the panel (shaker).

The two plots in Fig. 19 show the measured velocity at error sensor number 7 per unit excitation of the loudspeaker in the cavity between 0–1 (a) and 0–2 (b) kHz without control (solid line) and when the 16 decentralized feedback control units are implemented using a relatively high gain that guarantees stability (faint line). Compared to the experiment with only one control unit, larger reductions of the vibration level are achieved up to 2 kHz. In particular, as shown in Fig. 19(a), the two uncontrolled resonance frequencies at 70 and 177 Hz are now much more damped. Having 16 control units provides the larger control strength necessary to damp the low frequency natural modes that are well coupled with the volumetric response of the acoustic cavity underneath the panel. However even the 16 decentralized control units still find it difficult to control the other resonance frequency at 388, 510, 686, 844, 892 Hz. These are resonances generated by a strong coupling between a natural mode of the panel and a natural mode of the acoustic cavity that in order to be damped require even larger control authority than that provided by the 16 units. However, except for these modes, reductions from 5 to 20 dB are measured up to 1 kHz and reductions of about 6 dB are measured within a relatively larger number of narrow frequency bands at higher frequencies than in the case of a single active control unit.

The two plots in Fig. 20 show the measured velocity at error sensor number 7 per unit excitation of the shaker on the panel between 0–1 (a) and 0–2 (b) kHz without control (solid line) and when the feedback control system with compensator number 7 is implemented using a relatively high gain (faint line). These two plots indicate better results to those shown for the loudspeaker primary excitation in Fig. 19 with relatively larger reductions of the vibration level up to 2 kHz. Fig. 20(a) shows that also in this case the 16 channel control system produces larger damping effects than the single control unit, particularly for the resonances frequency at 70, 103, 183, 506 and 714 Hz where reductions from 10 to 20 dB are achieved. This interesting result is probably due to the fact that having 16 decentralized control units scattered over the panel produces a relatively larger control strength for many low frequency modes. In general, reductions from 5 up to 25 dB are measured between 0 and 1 kHz and reductions of about 8 dB are found for a wide frequency band between 1200 and 2000 Hz.

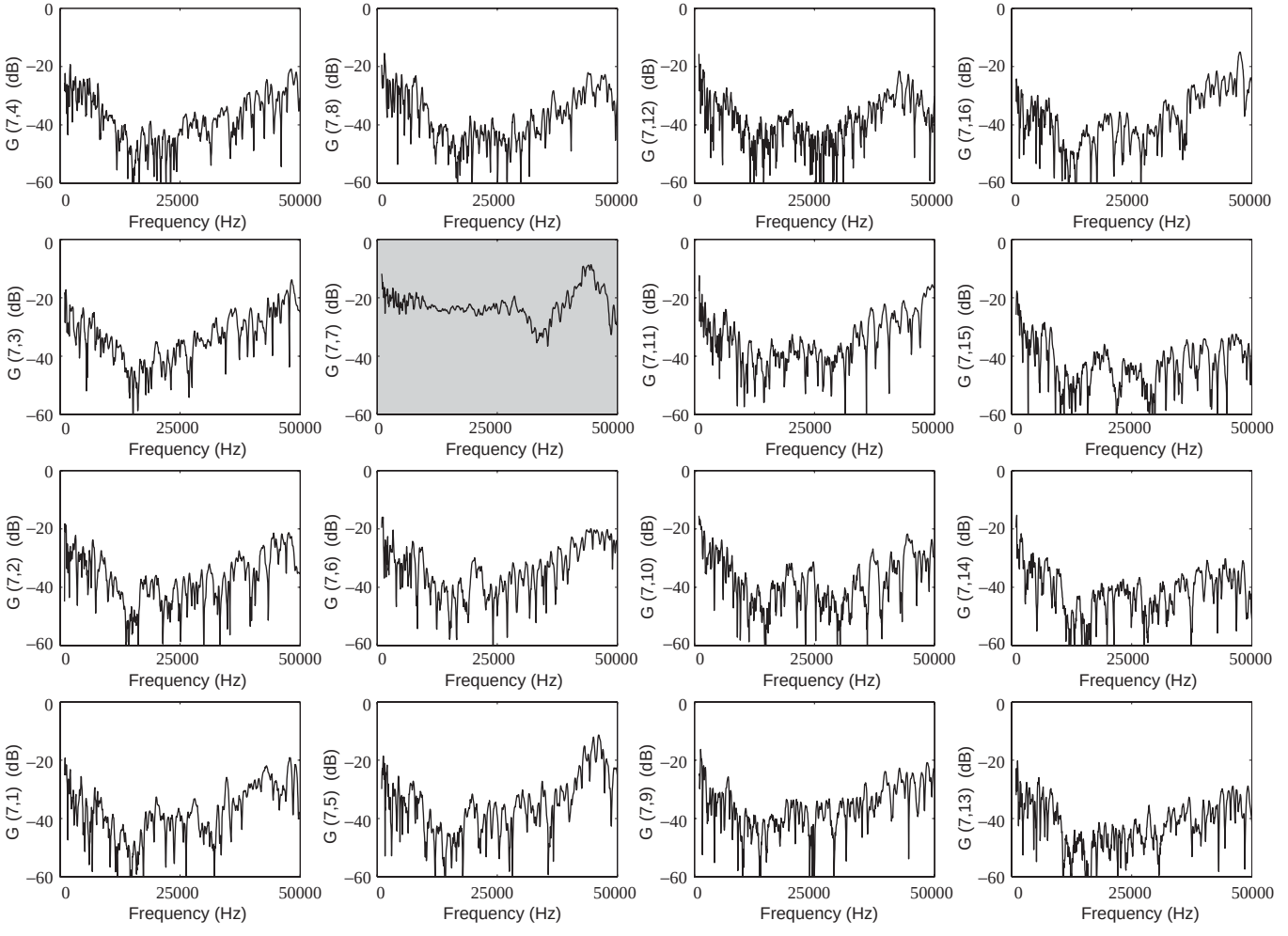

Fig. 17. Modulus of the measured frequency response functions between piezoceramic patch actuator number 7 and the 16 error sensors in a frequency range between 0 and 50 kHz. The shaded curve is for the sensor mounted on top of the actuator number 7.

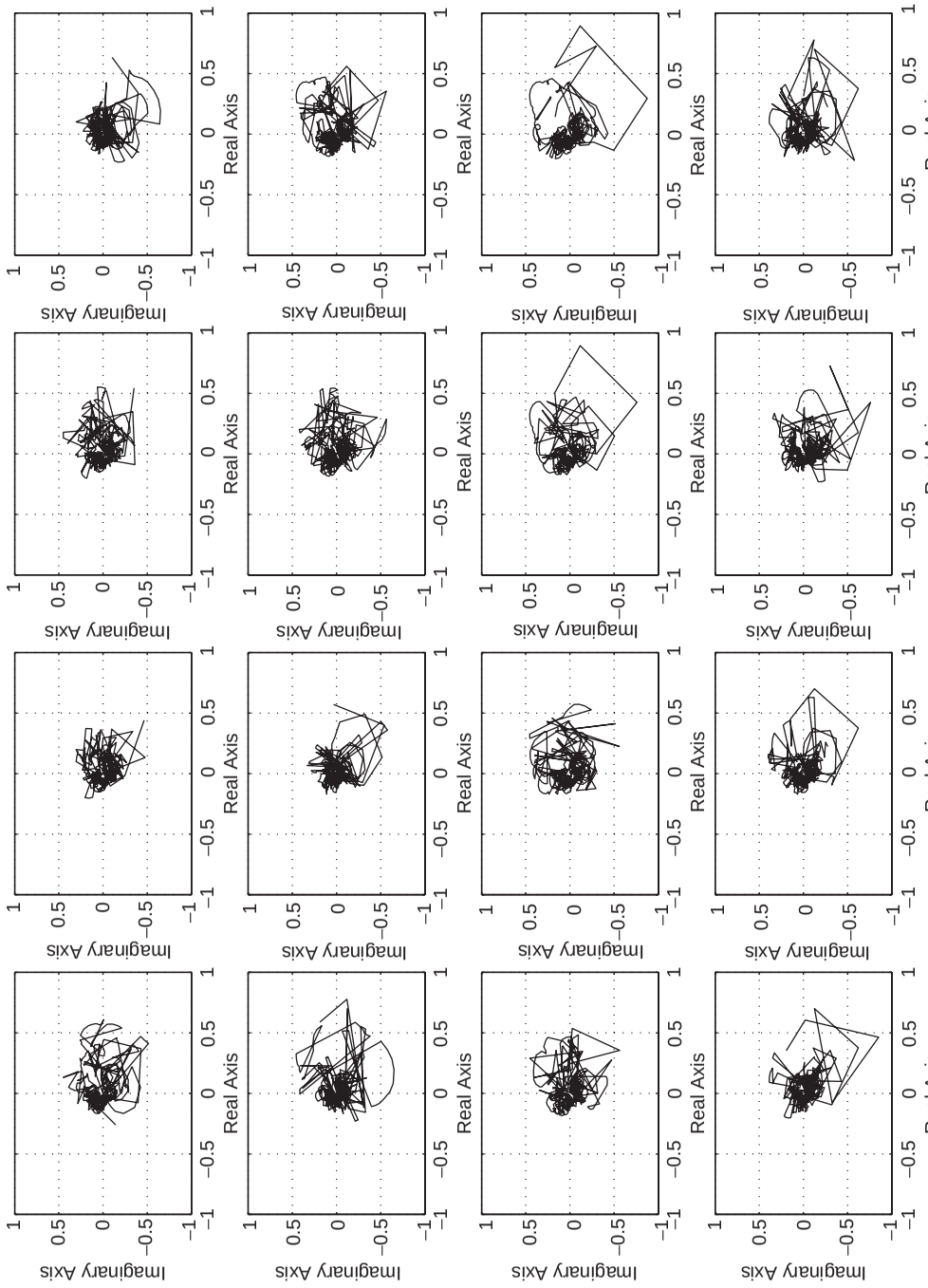

Fig. 18. Loci of the eigenvalues of the measured sensor–controller–actuator transfer matrix $\mathbf{G}(j\omega)\mathbf{H}(j\omega)$ between 5 and 50 kHz.

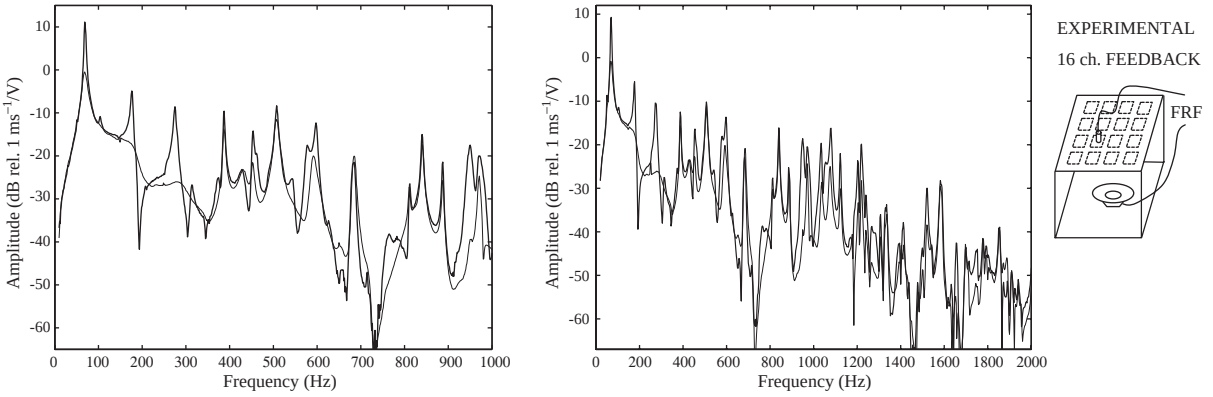

Fig. 19. Measured velocity at error sensor number 7 per unit excitation of the loudspeaker in the cavity between 0–1 (a) and 0–2 (b) kHz without control (solid line) and when the 16 decentralized feedback control systems with compensator are implemented (faint line).

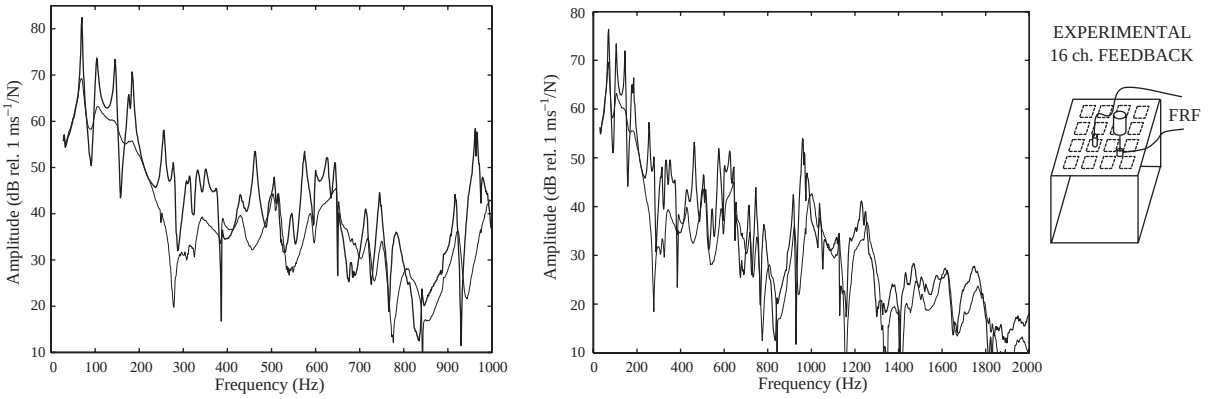

Fig. 20. Measured velocity at error sensor number 7 per unit excitation of the shaker on the panel between 0–1 (a) and 0–2 (b) kHz. without control (solid line) and when the 16 decentralized feedback control systems with compensator are implemented (faint line).

6. Concluding remarks

This paper summarizes the design study and implementation of 16 decentralized velocity feedback control systems embedded on a smart panel for the reduction of sound radiation/transmission. This work has been structured into three stages: first the analysis of the sensor–actuator response function; second, the design of the single channel velocity feedback controller when only one control unit is working and third, the implementation of the designed controller on the 16 control units of the smart panel. The analysis of the measured and simulated sensor–actuator response function has provided the following information.

1. At very low frequencies, below about 283 Hz, the response function is characterized by well separated resonant frequencies due to the panel natural modes while at higher frequencies the

dynamic effects of the sensor and actuator transducers become more and more important and tend to flatten down the response function because of their mass effect.
2. At relatively higher frequencies the sensor–actuator frequency response function is characterized by a relatively wide frequency band trough between 30 and 40 kHz and a crest between 43 and 46 kHz. This is due to the fact that the 16 accelerometers are a sort of single-degree-of-freedom neutralizer that reduces the vibration level at the measurement point in correspondence to its natural frequency. Since their resonance frequencies are uniformly spread between 35 and 42 kHz, then the wide-frequency trough and crest are found.
3. The sensor–actuator frequency response function is affected by a large phase shift above 10 kHz which is due to the fact that the accelerometer and the piezoceramic patch are not a truly collocated and dual sensor–actuator pair. It has been demonstrated that the cut-off frequency for a non-collocated behaviour can be raised by reducing the size of the actuator.
4. In general the actuation mechanism of the piezoceramic patch produces very few localized effects. The localized response of the panel becomes relatively complex only when the bending wavelengths are smaller than the dimensions of the piezoceramic patch actuator.

The design of the single channel velocity feedback control system when only one control unit is active has shown the following features.

1. When direct velocity feedback control is implemented the Nyquist plot has shown that the above-mentioned trough of the frequency response function occupies the negative real side and therefore, it allows relatively large gain margin to implement a stable controller with low spillover phenomena.
2. The gain can be further increased by 15 times when a phase-lag compensator is used.

Finally the implementation of the 16 decentralized control units has produced the following results.

1. Good low frequency control can be achieved with reductions of the measured velocity at the error sensor up to 15 or 20 dB at relatively low frequencies and of the order of 3–6 dB at higher frequencies up to 2 kHz.
2. However, the control system finds it difficult to damp down some resonance frequencies for three possible factors: first, the loading effect on the panel generated by the low frequency volumetric acoustic response of the cavity; second, the low spatial control authority of the actuator transducers for some of the resonant structural modes and third, the low control strength of the actuator transducers for well-coupled panel and cavity modes.

It is important to emphasize that the choice of testing the smart panel when mounted on a cavity is for practical reasons. Indeed this configuration has enabled an easy estimate of the sound radiation/transmission by the panel even though it has introduced the modal coupling between the cavity and the panel which is limiting the control performance at some resonance frequencies.

Acknowledgements

The work carried out by Mr Bianchi for this study is within the ''European Doctorate in Sound and Vibration Studies'' which is supported through a European Community Marie Curie Fellowship.

References

[1] A. Preumont, *Vibration Control of Active Structures*, 2nd Edition, Kluwer Academic Publishers, Dordrecht, 2002.
[2] P. Gardonio, E. Bianchi, S.J. Elliott, Smart panel with multiple decentralized units for the control of sound transmission. Part I: theoretical predictions, *Journal of Sound and Vibration* 274 (1–2) (2004) 163–192, this issue.
[3] S.J. Elliott, P. Gardonio, T.J. Sors, M.J. Brennan, Active vibroacoustic control with multiple local feedback loops, *Journal of the Acoustical Society of America* 111 (2) (2002) 908–915.
[4] S.E. Burke, J.E. Hubbard Jr., J.E. Meyer, Distributed transducers and collocation, *Mechanical Systems and Signal Processing* 7 (4) (1993) 765–770.
[5] J.Q. Sun, Some observations on physical duality and collocation of structural control sensors and actuators, *Journal of Sound and Vibration* 194 (5) (1996) 765–770.
[6] V. Jayachadran, J.Q. Sun, Unconditional stability domains of structural control systems using dual actuator–sensor pairs, *Journal of Sound and Vibration* 208 (1) (1997) 159–166.
[7] M.J. Balas, Direct velocity feedback of large space structures, *Journal of Guidance and Control* 2 (1979) 252–253.
[8] Postelwhite, *Adaptive Structures*, 1st Edition, Wiley, New York, 1998.
[9] P. Gardonio, E. Bianchi, S.J. Elliott, Smart panel with multiple decentralized units for the control of sound transmission. Part III: control system implementation, *Journal of Sound and Vibration* 274 (1–2) (2004) 215–232, this issue.
[10] C.K. Lee, Theory of laminated piezoceramic plates for the design of distributed sensor/actuators. Part I: governing equations and reciprocal relationships, *Journal of the Acoustical Society of America* 87 (3) (1990) 1144–1158.
[11] C.R. Fuller, S.J. Elliott, P.A. Nelson, *Active Control of Vibration*, 1st Edition, Academic Press, London, 1996.
[12] E. Bianchi, Smart Panel with an Array of Decentralized Control Systems for Active Structural Acoustic Control, PhD Thesis, University of Southampton, 2003.